

# Beyond Convolutions: A Novel Deep Learning Approach for Raw Seismic Data Ingestion

Zhaozhuo Xu<sup>\*1</sup>, Aditya Desai<sup>\*1</sup>, Menal Gupta<sup>2</sup>, Anu Chandran<sup>2</sup>, Antoine Vial-Aussavy<sup>2</sup> and Anshumali Shrivastava<sup>1</sup>

<sup>1</sup>Department of Computer Science, Rice University

<sup>2</sup>Shell International E&P, Inc

*zx22, apd10, anshumali@rice.edu*

*Menal.Gupta, Anu.Chandran, a.vial-aussavy@shell.com*

## Abstract

Traditional seismic processing workflows (SPW) are expensive, requiring over a year of human and computational effort. Deep learning (DL) based data-driven seismic workflows (DSPW) hold the potential to reduce these timelines to a few minutes. Raw seismic data (terabytes) and required subsurface prediction (gigabytes) are enormous. This large-scale, spatially irregular time-series data poses seismic data ingestion (SDI) as an unconventional yet fundamental problem in DSPW. Current DL research is limited to small-scale simplified synthetic datasets as they treat seismic data like images and process them with convolution networks. Real seismic data, however, is at least 5D. Applying 5D convolutions to this scale is computationally prohibitive. Moreover, raw seismic data is highly unstructured and hence inherently non-image like. We propose a fundamental shift to move away from convolutions and introduce SESDI: Set Embedding based SDI approach. SESDI first breaks down the mammoth task of large-scale prediction into an efficient compact auxiliary task. SESDI gracefully incorporates irregularities in data with its novel model architecture. We believe SESDI is the first successful demonstration of end-to-end learning on real seismic data. SESDI achieves SSIM of over 0.8 on velocity inversion task on real proprietary data from the Gulf of Mexico and outperforms the state-of-the-art U-Net model on synthetic datasets.

## 1 Introduction

Seismic reflection data, obtained via reflection seismology Waters & Waters (1981), is a dominant information source to understand the earth's subsurface. Figure 1b shows a typical setup for re-

flexion seismology. It uses apparatus such as air guns (sources) to generate pressure waves on the earth's surface. These waves encounter geological contrast in the subsurface and reflect back to the multiple geophones (receivers) positioned on the surface. This time-dependent recording of amplitudes by receivers constitutes the seismic data. The recording of each source, receiver pair is called a trace. The positions(x,y coordinates) of sources and receivers are referred to as acquisition geometry. Each trace is associated with additional metadata such as the signature of disturbance, etc. Even ignoring this metadata, the trace is at least five-dimensional (surface coordinates for both source and receiver and time). A typical seismic survey is extensive (100 km  $\times$  100km), with each 1km x 1km patch having tens of thousands of traces resulting in data sizes of 10-100 terabytes. Conventionally, seismic data is processed using wave propagation physics to invert for relevant earth properties. We present a novel Deep learning based SDI approach, denoted as Set Embedding based SDI (SESDI), that efficiently ingests raw seismic data directly with applicability in any seismic processing workflow. This paper selects seismic velocity inversion, one of the most crucial subsurface properties, as a case study for SESDI. SESDI benefits effective analysis of seismic data in environmental applications such as earthquake understanding Sergeant et al. (2016); Julian & Foulger (1996); Arora et al. (2010), groundwater investigation Zelt et al. (2006) and hydrocarbon exploration Alsadi (2017).

**Expensive seismic processing workflows:** Traditional state-of-the-art methods of processing seismic data consume significant resources and time Onajite (2013). Figure 1a shows broader steps in traditional workflow commonly used in the "Big Oil" industry. It is well known Le Ravalec et al. (2012) that each of the sequential steps in traditional workflows require

<sup>\*</sup>Equal contributions.

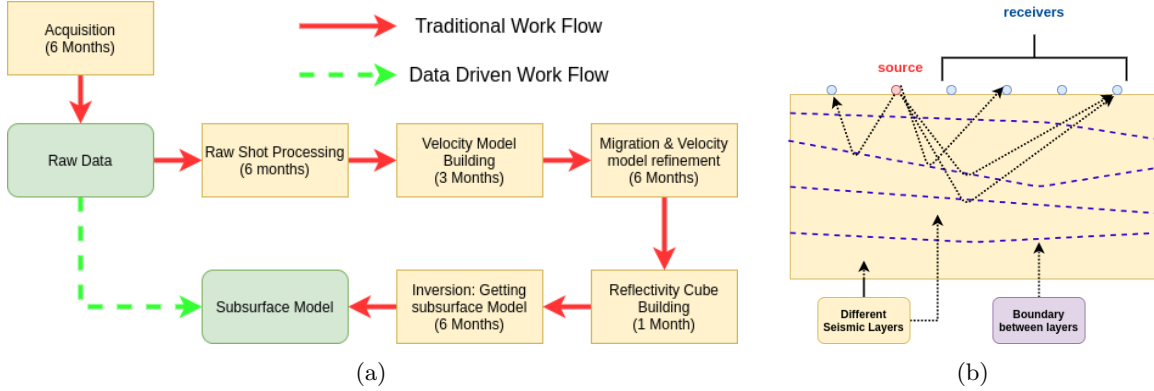


Figure 1: **Left:**Traditional workflow involved in seismic processing of raw data to getting a subsurface model. It requires approximately over an year time to generate a subsurface image. Data-driven workflows try to bypass this tedious process by directly predicting subsurface model from raw data. **Right:** Reflection Seismology for collecting seismic data: Mechanical Perturbation (sound wave) created at source, propagates through layers of earth and reflects subsurface boundaries. The receivers record amplitude time-series information.

several months. This time inefficiency is primarily due to their dependence on human expertise to process vast amounts of raw data. With the increasingly comprehensive and complex seismic data generated by advanced sensing technology, traditional workflows prove to be more expensive than ever. Hence, there is an urgent need to devise techniques to reduce human involvement in seismic processing.

**Promise of deep Learning (DL):** The data-driven approaches Fichtner (2010); Lin & Huang (2014a,b, 2015) are progressively sought alternative to improve seismic workflows' efficiency. Data-driven deep learning (DL) approaches aim to learn a non-linear mapping from the raw seismic data to the final subsurface image evading most of the time-consuming sequential steps in traditional workflows. With the fast inference of DL models, data-driven approaches can potentially reduce workflows' duration from months to minutes. Therefore, it is not surprising that DL based workflows in seismic processing are getting the attention and investment they deserve. Dramsch & Lüthje (2018); Li et al. (2019); Griffith et al. (2019); Zheng et al. (2019); Yang & Ma (2019); Sun et al. (2020); Wu & Lin (2018); Rojas-Gómez et al. (2020); Araya et al. (2017, 2018)

**Convolutions in data-driven processing** Treating parts of raw seismic data as images is standard in the oil industry and geophysics community. Undoubtedly, image is the most convenient and interpretable representation of complex data. The recent data-driven research, inheriting the image-bias from traditional practices and inspired by the success of convolutions in computer vision, attempts to process the raw seismic data as images and apply convolution based networks to ingest them. Wu & Lin (2018);

Dramsch & Lüthje (2018); Di et al. (2018); Zheng et al. (2019); Yang & Ma (2019); Sun et al. (2020); Rojas-Gómez et al. (2020).

**Limited success of deep learning in real seismic processing:** Current DL based SDI with CNN architecture suffers severely from two major constraints 1) Real seismic data is at least 5 dimensional. Applying 5D convolutions to the extensive seismic data is computationally infeasible. 2) Real seismic data collection is highly irregular and unstructured (see Figure 2). However, CNNs' strong requirements on structured data limit their application in regular consistent acquisition geometry. Thus, to the best of our knowledge, most CNN based SDI approaches are prohibitive to real seismic settings. These methods' current success is produced on simulations over 2D velocity patches with regular acquisition geometry (see Figure 5). Here, sources and receivers are uniformly distributed on the surface and each receiver listening to every source. The gap between simulation and practice is too wide to extend these methodologies to practical environmental applications.

#### Major contributions in the paper

- We propose a fundamental shift to move away from convolutions in data-driven seismic processing.
- We introduce SESDI approach which 1.) redefines the seismic inversion problem on terabytes of data into the auxiliary task of predicting small blocks of property models from their contextual traces. Thus making training and inference of deep learning models on real data feasible. 2) We provide a deep semantic embedding model for a set of contextual traces that is robust to highly irregular acquisition geometry. 3) SESDI approach is a SDI approach; the embedding obtained for a context can be used

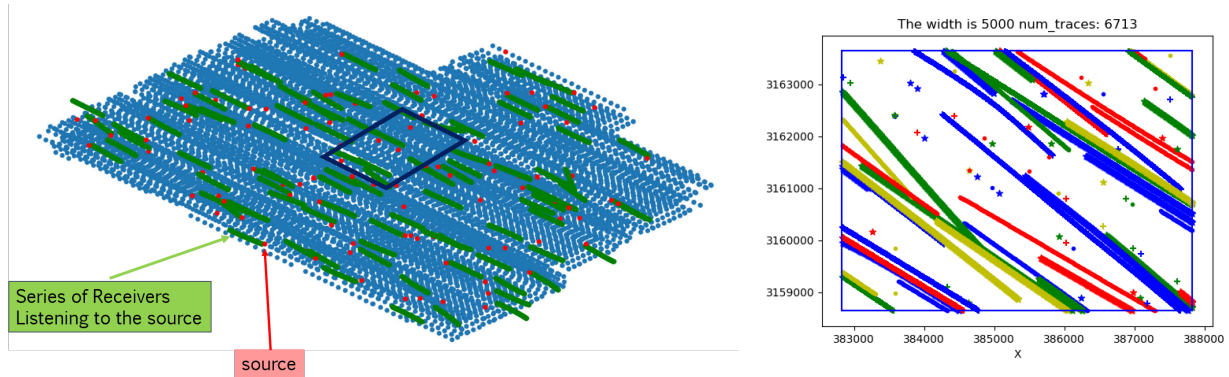


Figure 2: Irregular Acquisition in real SDI. **Left:** A top view of a real survey. The survey area is large (around  $100\text{Km} \times 100\text{Km}$ ) and the streamer (in marine survey) moves across the area to collect data. The blue dots represent the source points in the survey. Red dots and nearby green segments refer to a pair of source and series of receivers. We focus on a particular area to predict the subsurface properties. **Right:** Details at the acquisition over a  $5\text{Km} \times 5\text{Km}$  area. Different colors and symbols are used to identify pairs of source and receiver lines. The real acquisition is highly irregular emphasizing the oversimplification of data used in current convolution models. Seismic data courtesy of TGS.

- for any downstream task such as velocity inversion.
- We believe, SESDI is the first-ever data-driven workflow that can reasonably ingest real data and provide geologically sound results. In the experiments on real proprietary data from the survey on the Gulf of Mexico, we achieve a SSIM similarity (0-worst, 1-best) of over 0.8 on predicting 3D velocity model cubes.
- We outperform state-of-the-art U-Net model with just MLP functional blocks on synthetic datasets, suggesting re-thinking the need for convolutions for SDI.

## 2 Background

### 2.1 Seismic Data and Associated Applications

For environmental applications such as hydrocarbon exploration and groundwater investigation, geophysicists aim to create a subsurface property model. Generally, the property model map is stored as a discretized 3d cube with the uniform value per partition.

**Definition 1 (Subsurface Property Model).** *Subsurface property model is defined as a map  $\mathcal{P} : \mathbb{R}^3 \rightarrow \mathbb{R}^k$  which maps each point in the subsurface to a tuple of properties like density, shear modulus bulk modulus, etc*

Reflection Seismology Waters & Waters (1981) is used to collect information about the subsurface which is

used to construct property model. We restrict our discussion to the marine survey in this paper.

#### 2.1.1 REFLECTION SEISMOLOGY:

As shown in Figure 1b, a source and a set of receivers are positioned on the surface of earth. A mechanical perturbation is created using air guns at the source. The pressure waves thus generated travels through the subsurface. They refract and reflect at different layer boundaries in the subsurface. The reflected pressure waves that reach the receivers are recorded to generate a time-series data. Hence, each source shot and receiver pair is associated with a 1D time series data called the *trace* which is formally defined as

**Definition 2 (Trace Data ( $u$ )).** *Given a time duration  $t$ , and a frequency  $f$ , a trace at a location  $x$  on surface is defined as the sequence  $\{u(t_i, x)\}_{i=1}^{t \cdot f}$  of acoustic pressure sensed at  $x$  at time  $t_i$ , where  $t_i$  is the  $i^{\text{th}}$  time sample when sampling with frequency  $f$  for time  $t$ .*

**Definition 3 (Geometry-Aware Trace ( $t$ )).** *The trace data,  $u$ , along with its (source, receiver) locations,  $q$ , together constitute a geometry-aware trace:  $t = (u, q)$ . We use functions  $u = \mathcal{D}(t)$  and  $q = \mathcal{A}(t)$  to extract trace data and location information respectively from the trace*

In a typical survey, a source is located on the streamer and long cables with equidistant receivers are attached to the streamer. The streamer moves over the

area of interest and collects a large set of traces for different (source, receiver) pairs. If the total number of traces obtained from the survey is  $N$ , we define raw-data as the set of all geometry-aware traces. Specifically raw-data =  $\{t_i\}_{i=1}^N$ . The set of (source, receiver) locations associated with the collected traces is referred to as the acquisition geometry that formally defined as

**Definition 4 (Acquisition Geometry( $\mathbb{A}$ )).** *Acquisition Geometry is defined as the set  $\{\mathcal{A}(t)|t \in \text{raw-data}\}$*

Traces are consequence of the propagation and reflection of pressure wave through the subsurface. The propagation of reflected waves is generally modelled by the Acoustic Wave Equation, defined as below

**Definition 5 (Acoustic Wave Equation).** *Given a position vector  $x$ , spatially varying wave velocity denoted as  $v(x)$ . Provided with a seismic source  $q_s(t, x)$  located as  $x_s$ . The acoustic pressure  $u(t, x)$  in time  $t$  is determined by:*

$$m \frac{\partial^2 u(t, x)}{\partial t^2} - \nabla^2 u(t, x) + \eta \frac{\partial u(t, x)}{\partial t} = q_s(t, x) \quad (1)$$

where  $m(x) = v^{-2}(x)$  is the squared slowness at  $x$ ,  $\eta(x)$  is the space-dependent dampening parameter for the absorbing boundary layer Cerjan et al. (1985) and  $\nabla^2$  is the laplacian operator.

### 2.1.2 APPLICATIONS OF SEISMIC DATA

The final aim of seismic processing is to obtain a subsurface property model. This problem is referred to as the seismic inversion problem stated formally below. This property model can then identify the rock and fluid types in the subsurface.

**Problem 1 (Seismic Inversion ).** *Given a region of interest  $S \subset R^d$ , set of traces  $T$  and associated Acquisition Geometry  $\mathbb{A}$ , Seismic Inversion(SI) is defined as the problem of getting the property model  $\mathcal{P}$*

The property here can be any set of elastic properties, intermediate velocity or reflectivity index, etc. We use the term *property* in the most general manner. The subsurface region of interest,  $S$ , in problem definition 1 can be 2D or 3D space. Accordingly, the inversion problems are categorized as 2D or 3D problems. 2D problems generally appear in synthetically generated datasets.

## 2.2 Relevant Prior Work

**Traditional approaches** Yilmaz (2001): Traditionally SDI for seismic workflows comprises a series of

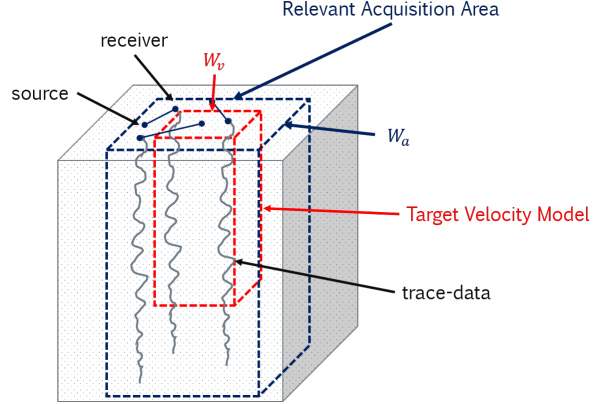


Figure 3: Construction of context for a particular property model block placed near surface of earth.

sequential steps involving computer-assisted human analysis. Generally, these steps are physics-driven. An example of workflow with approximate timelines is shown in figure 1a. Raw shot processing cleans up the data by removing unintended noises that appear in the data. It includes sequential steps like de-noising, de-signature, de-multiple etc Yilmaz (2001); Mandelli et al. (2019); Calderon Agudo et al. (2016); Van Der Neut et al. (2011). The clean data is used to generate a velocity model of the subsurface using techniques of tomography Nolet (1987); Shapiro et al. (2005) or full-waveform inversion Virieux & Operto (2009); Brossier et al. (2009). The velocity model is then refined iteratively by migrating the waves and computing errors like residual move out Xie & Yang (2008). Once a refined velocity model is obtained, it is used to build a reflectivity cube of the subsurface. This cube is then inverted to obtain elastic properties of the subsurface (subsurface property model). Types of rocks and fluids in the subsurface are identified by analyzing the property Model. Each of these steps require involvement of domain experts to guide the inversion to an effective and applicable solution. These procedures extend the overall process to as lengthy as a year. For a detailed discussion on these steps, we refer the readers to Yilmaz (2001).

**Recent DL approaches:** Though the application of data-driven methods to seismic processing dates back to Nath et al. (1999), there has been renewed interest since the success of deep learning Goodfellow et al. (2016). The data-driven methods Wu & Lin (2018); Yang & Ma (2019) aim to utilize the strength of deep learning Goodfellow et al. (2016) to exploit the available extensive complex seismic data fully. Most existing methods formulate Problem 1 as an image segmentation problem and utilize convolutional neural networks (CNN) Ronneberger et al. (2015); Chen et al. (2017). In this formulation, the traces

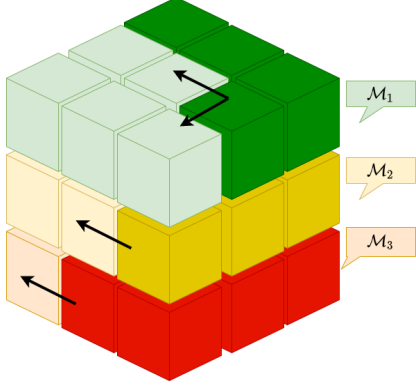


Figure 4: Creating entire property model using different learning models at different depths with each model traversing entire horizontal surface predicting one block at a time.

are combined as multi-channel images and the corresponding subsurface property model is regarded as a segmentation mask. Then CNN architectures such as U-Nets Zheng et al. (2019); Yang & Ma (2019); Sun et al. (2020) or encoder-decoders Wu & Lin (2018); Rojas-Gómez et al. (2020) are applied to learn a non-linear mapping between image-mask pairs. As stated earlier, these approaches do not scale to real data.

### 3 SESDI: Set Embedding based Seismic Data Ingestion

#### 3.1 Decomposition of Original Problem

The raw data for a typical survey measures up to several terabytes, while the discretized output property model of the subsurface beneath the survey area is in several gigabytes. It is prohibitive to learn a mapping that directly attempts to ingest terabytes of seismic data and produce a big property model. Unlike current state-of-the-art methods, SESDI is designed to work for real data. SESDI surmounts the problem of scale by breaking this task into an achievable auxiliary task of predicting small property model blocks using the contextual traces and then stitching them together to obtain the complete property model. One can draw an analogy to NLP models on machine document translation. Instead of learning a complete mapping between two documents, state-of-art techniques design a model to predict the next word given the current context and use this to translate the entire document. Similarly, SESDI predicts a property model block by considering the traces that appear around it.

Let the property model block of size  $w_p \times w_p \times d$  with its midpoint located at a particular location, say  $q$ , in 3D space be denoted by  $\mathcal{P}(q, w_p, d)$ . We define the

context for such a block, shown in figure 3, formally,

**Definition 6 (Context  $\mathcal{C}(q, w)$ ).** The context,  $\mathcal{C}(q, w)$ , at a point  $q$ , parameterised by width  $w$  is defined as the set of geometry-aware traces whose acquisition (source and receiver locations) lie inside  $Area(q, w)$ , i.e. the area  $w \times w$  centered at  $(q.x, q.y)$

$$\mathcal{C}(q, w) = \{t | t \in \text{raw-data}, \mathcal{A}(t) \in Area(q, w)\}$$

SESDI aims to learn a mapping,  $\mathcal{M}$ , between  $context(q, w_a)$  and property model block  $p(q, w_p, d)$ . The scale of this learning problem is much lesser as compared to the original problem, making it feasible to train a model efficiently. SESDI proposes to learn different mappings for different depths. For example if the total depth of complete property model is  $D$  and we choose to predict model blocks of depth  $d$ , then SESDI proposes to learn  $\lceil D/d \rceil$  mappings  $\{\mathcal{M}_i\}_{i=1}^{\lceil D/d \rceil}$ . With the help of  $\lceil D/d \rceil$  models, SESDI can predict the entire property model as shown in figure 4. Specifically, in order to predict property at a arbitrary location, say  $q$ , in the subsurface, we would use the the mapping  $\mathcal{M}_{\lceil q/d \rceil}$  with context  $context(q, w(\lceil q/d \rceil))$  and then locating the point  $q$  inside the predicted block. The width of context  $w$  should increase when predicting property at higher depth. Hence, we use  $w(\lceil q/d \rceil)$  to make the dependence explicit.

#### 3.2 Learning a Mapping $\mathcal{M}$

Let us focus on predicting the property model block at a specific depth.

##### 3.2.1 INFORMATION-ALIGNED TRACE EMBEDDINGS

For a particular property model block,  $\mathcal{P}(q, w_p, d)$ , let the context block be  $\mathcal{C}(q, w)$ . Let  $\mathcal{C}(q, w) = \{t_i\}_{i=1}^n$ . Trace data,  $\mathcal{D}(t)$ , is a sequential amplitude recording of pressure wave measured at receiver. The receiver catches the reflected waves from different depths and directions. The recorded amplitude is a superposition of all waves that reach the receiver simultaneously with lesser contributions from waves reflected from faraway points. Hence, each trace captures relevant information about the entire subsurface. In this respect, the raw data is a collection of highly redundant and correlated traces containing overlapping pieces of information about the entire subsurface. SESDI has to align the information of these pieces before combining them to generate property model block. The information of acquisition of a trace  $t$ ,  $\mathcal{A}(t)$  is important to align the semantic information from different traces correctly and consistently. In SESDI,

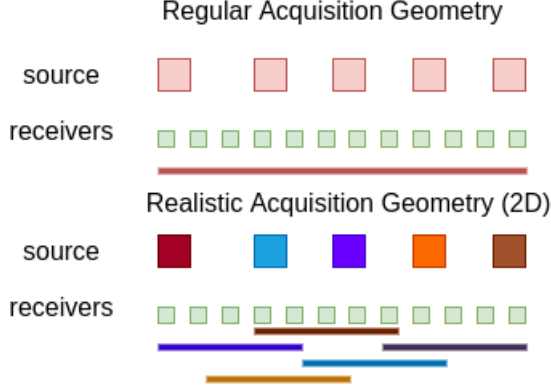


Figure 5: Regular AG used in synthetic datasets is to have sources and receivers uniformly distributed on surface and have every receiver listen to every source. Realistic AG for 2D is designed to mimic Real acquisition. Here, randomly sampled contiguous segments of receivers are made to listen to each source. The color shows the pairings of receivers and sources.

we achieve this aligned semantic embedding by first projecting the trace-data  $\mathcal{D}(t)$  and its acquisition  $\mathcal{A}(t)$  independently into intermediate high dimensional space, combining them and projecting them in the final target embedding space. Formally,

$$\mathcal{E}(t) = \phi(t) = \mathcal{F}_t([\mathcal{F}_{aq}(\mathcal{A}(t)), \mathcal{F}_d(\mathcal{D}(t))])$$

The resulting bag  $\{\mathcal{E}(t_i)\}_{i=1}^n$  is a set of information-aligned trace embeddings. In our experiments on seismic data, we use Multi layer Perceptrons (MLPs) for the functional blocks  $\mathcal{F}_{aq}$ ,  $\mathcal{F}_d$  and  $\mathcal{F}_t$ .

### 3.2.2 REPRESENTATION OF CONTEXT $\mathcal{C}$

In a real survey (Figure 2), the acquisition geometry and the number of traces in a context  $\mathcal{C}(q, w)$  change with changing location  $q$  of the context. Due to this irregularity of traces across different contexts, it is impossible to impose specific structural formulations such as convolution or concatenation on the trace embeddings. To tackle these issues, we propose a set formulation to learn a high dimensional representation of the context  $\mathcal{C}(q, w)$ . If  $\mathcal{C}(q, w) = \{t_i\}_{i=1}^n$  then, we define the context embedding as,

$$\mathcal{E}(\mathcal{C}(q, w)) = \frac{1}{n} \sum_{i=1}^n \phi(t_i)$$

where  $\phi(t_i) = \mathcal{E}(t_i)$  is the information-aligned embedding of the trace  $t_i$  as defined in 3.2.1. Alignment of trace embeddings is of key significance in this formulation.

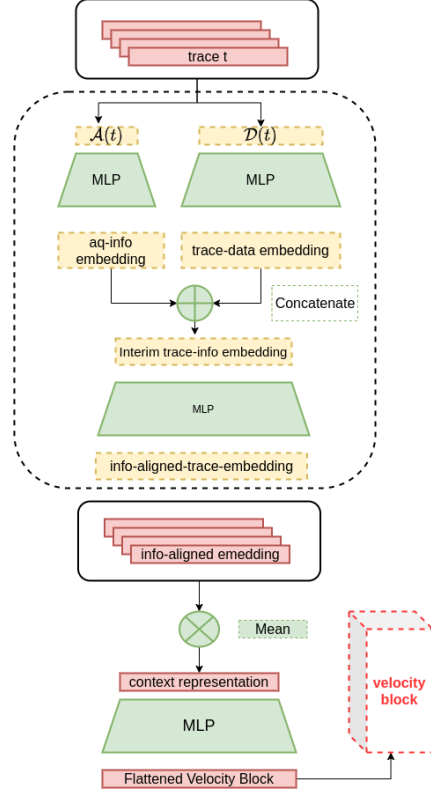


Figure 6: SESDI Model Architecture

### 3.2.3 DOWNSTREAM TASKS

Once a context representation is obtained, we can now use this to predict any property we desire, such velocity model, reflectivity model or even elastic properties of the subsurface. The property model is predicted by processing the context embedding using a function  $\rho$ .

$$\hat{\mathcal{P}} = \rho(\mathcal{E}(\mathcal{C}(q, w)))$$

Again, we implement  $\rho$  as a MLP. We learn all the functional blocks in an end-to-end fashion. Hence,

$$\hat{\mathcal{P}} = \rho\left(\frac{1}{n} \sum_{i=1}^n \mathcal{F}_t([\mathcal{F}_{aq}(\mathcal{A}(t_i)), \mathcal{F}_d(\mathcal{D}(t_i))])\right)$$

Coincidentally, this formulation also agrees with a recent paper on processing sets via deep learning Zaheer et al. (2017). An overview of SESDI model is shown in Figure 6

### 3.2.4 TRAINING DATA

$(\mathcal{C}(q, w), \mathcal{P}(q, w_p, d))$  is a training data sample for training a mapping  $\mathcal{M}$  of depth corresponding to  $q$ . Given a huge survey area, we can sample different points  $q$  in the subsurface to generate multiple data points. Sometimes the availability of labeled real

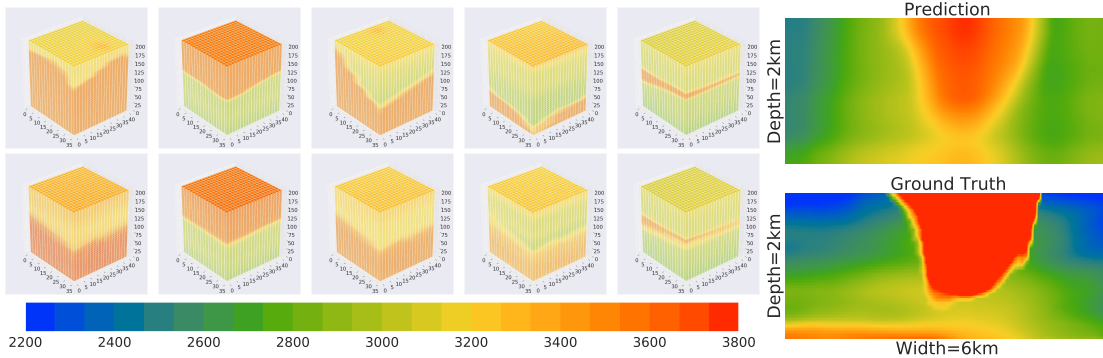


Figure 7: Visualization of prediction on GulfM-20 Dataset. **Left:** Top: ground-truth velocity cube, Bottom: predicted velocities. **Right:** cross-section visualization of inference on whole area. We want to stress that generating the above image from raw data via traditional methods takes several months because of the complex large scale data. Seismic data courtesy of TGS.

data is scarce. In such cases, we can sub-sample the context to generate more distinct training data points. Specifically, if  $(\mathcal{C}, \mathcal{P})$  is a data point for training, then so is  $(c, \mathcal{P})$  for every  $c$  in power set of  $\mathcal{C}$ , i.e.  $c \in 2^{\mathcal{C}}$ . We also observe that generalization of the model is better when trained with augmented subsampled data. Because SESDI is robust to different number of traces in the context, we can even use subsampling to improve the model’s inference time in seismic processing.

### 3.3 Benefits of SESDI

**Large scale property model prediction:** With the help of auxiliary task of contextual property model block, SESDI can efficiently predict a large scale property model.

**Robust to varying and irregular acquisition geometry:** SESDI alleviates the issue of highly irregular acquisition and seamlessly works with varying amounts of data.

**Scalable to k-dimensional real data** Unlike current SDI approaches, it scales easily to 5-dimensional real data. SESDI, with its information-aligned trace embeddings can quickly ingest even higher dimensional seismic data obtained by adding more meta-details to each trace.

**Does not overfit even under scarce data** Labeled data in seismic tasks can be scarce. However, with the SESDI approach of generating data, we can create exponentially more distinct training samples from a small sample in data. (see 3.2.4). Training model using this sampling approach prevents the model from overfitting. For example, SEGSalt data has 130 training samples, but the SESDI model with sampling technique does not overfit even when we run the model for over 1200 epochs. (see figure 9)

## 4 Application and Empirical Results

We evaluate the SESDI approach against the competing methods on the velocity inversion problem

### 4.1 Baselines

- **U-Net** Yang & Ma (2019) is the state-of-the-art model in recent literature for data-driven seismic processing. Also, it is the only model that was evaluated on a publicly available SEGSalt data\*. Therefore, we choose this opensource Yang & Ma (2019) implementation as the representative for U-Net.
- **Set-Transformer** Lee et al. (2019) is the state-of-the-art model that introduce multi-head attention mechanisms on set representation. It has demonstrated its superiority in point cloud classification and anomaly detection.

The details on training strategies and hyper-parameters of these models can be found in supplement.

### 4.2 Datasets

To extensively evaluate SESDI against competing approaches, we carefully select the following datasets.

- **SEGSalt:** (small, regular, 2D Velocity). SEGSalt is a small scale, 2D velocity prediction dataset with regular acquisition (Fig.5). SEGSalt is an ideal dataset for the CNN-based U-net model used in Yang & Ma (2019) and is publicly available. We choose this data set to compare against U-net at its best.

**Data generation:** This data is generated by first designing 2D velocity models and then running forward wave propagation using tools like Devito

\*<https://wiki.seg.org/wiki/SEG>

Datasets	SEGSalt			RS-SEGSalt			GulfM-10	GulfM-20
Models	U-Net	Set-Transformer	SESDI	U-Net	Set-Transformer	SESDI	SESDI	SESDI
$\mathcal{L}_1$	196.82	232.78	<b>163.77</b>	-	294.76	<b>162.79</b>	135.27	164.99
PSNR	14.64	14.21	<b>16.65</b>	-	14.90	<b>16.68</b>	32.34	26.95
SSIM	0.45	0.40	<b>0.47</b>	-	0.34	<b>0.41</b>	0.82	0.75

Table 1: Summary of results of SESDI and baselines on all the four datasets.

Louboutin et al. (2019) Luporini et al. (2018) to obtain seismic traces. The acquisition geometry is regular: distributing 29 sources and 301 receivers uniformly along the surface line with each receiver listening to each source. For details of data generation, refer to the supplement.

- **RS-SEGSalt, Realistically-Sampled SEGSalt:** (small, irregular, 2D Velocity) RS-SEGSalt is obtained from SEGSalt by tweaking sampling the acquisition to make it more realistic. The way to sub-sample the traces is shown in figure 5. With such a simple tweak towards real data, the U-Net model breaks and cannot be applied.

**Data generation:** For each sample in SEGSalt for each epoch, we randomly sample a random fraction of contiguous traces. For experiments, we use a fraction uniformly sampled between  $(0.7 \pm 0.25)$  and then choose the contiguous strips of receivers at a uniformly random location.

- **GulfM-10 and GulfM-20**( real, enormous, highly irregular, 3D Velocity) These are raw, noisy datasets that we generate directly from real sensors obtained from a Big-Oil company without preprocessing steps like scaling, denoising, imputations, etc. This dataset contains missing values and highly irregular acquisition geometry, as shown in Figure 2. The data scale is also immense (  $100\text{Km} \times 100\text{Km}$ ) survey area). Due to the large scale, irregular geometry, this data set cannot be used by U-Net. We test set-transformer and SESDI on the auxiliary task of contextual velocity block prediction. We also show results on big block predictions by applying a sequence of contextual predictions and stitching together an image.

**Data generation:** For the task of contextual prediction, we sample data points as described in 3.2.4. The difference between GulfM-10 and GulfM-20 is the height of the target velocity block. GulfM-10 and GulfM-20 have velocity blocks with height 10% (1Km) and 20%(2Km) of the total velocity model, respectively. The block width and context width in both cases are 1Km and 5Km.

### 4.3 Metrics:

To evaluate the models, we use the following three metrics widely used in recent work on data-driven seis-

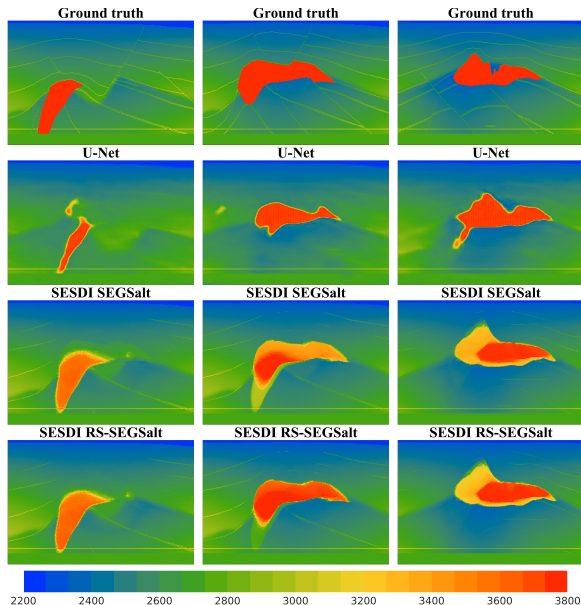


Figure 8: Visualization of Prediction on SEGSalt Dataset : The prediction results for U-net vs SESDI model. SESDI performs particularly well when trained on RS-SEGSalt data. Also, SESDI model is robust to irregularities in the acquisition.

mic processing Yang & Ma (2019); Wu & Lin (2018); Rojas-Gómez et al. (2020); Araya-Polo et al. (2018). Namely,  $\ell_1$  Loss (lower is better) , PSNR Huynh-Thu & Ghanbari (2008)(higher is better) and SSIM Wang et al. (2004)(higher is better).  $\ell_1$  loss is  $l_1$  metric applied to (input,output) images. SSIM is a structural similarity score widely used to measure the quality of images. PSNR (Peak Signal to noise ratio) is used to measure image reconstruction quality.

### 4.4 Results:

We provide results in various forms:

- **Performance on Metrics (Table 1)** : lists the performance of all the models on all the datasets on all metrics.
- **Metric evolution and Robustness ( Fig. 9)**: top panel shows the evolution of metrics. The bottom panel shows the performance of the SESDI model trained on RS-SEGSalt when used for inference on different sizes of the sampled data.
- **Visualization (Fig. 7, 8)** . Fig. 8 Shows the visualization of different models on SEGSalt. The



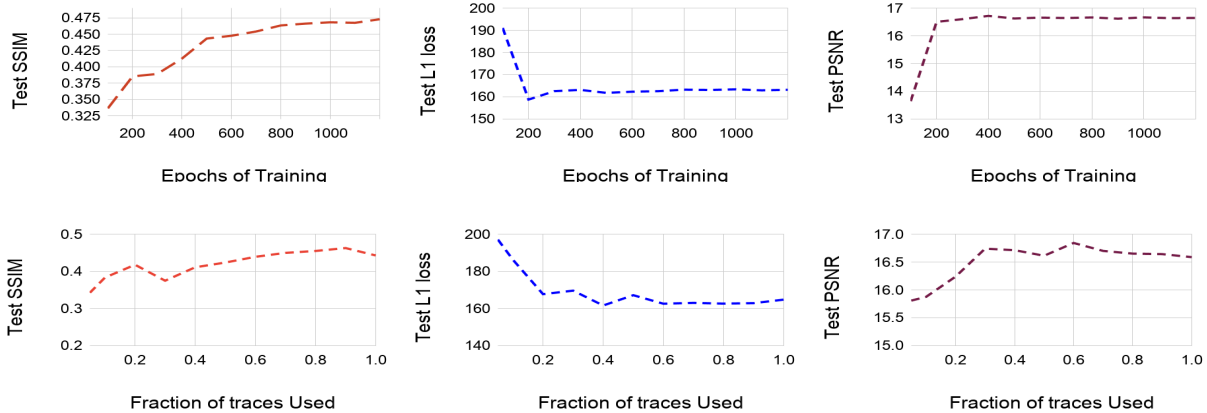


Figure 9: **Above:** Evolution of metrics SSIM,  $\mathcal{L}_1$  loss and PSNR on test SEGSalt dataset as the training progresses to 1200 epochs. As can be seen SSIM always improves and  $\mathcal{L}_1$  loss, PSNR achieve stable values. For elaboration on metrics see Experiments section. Model is trained with 0.8 fraction of traces. **Below:** Comparison on test performance when different fractions of traces is used for inference

entire test data visualization is presented in the supplement. We also show the performance of SESDI model trained on RS-SEGSalt data and inferred on SEGSalt. In Fig. 7, we show some visualisation on contextual block prediction task (left). Also, we run inference on larger blocks of velocity and show visualization for the same (right). Details of visualization are presented in the appendix.

#### Key Highlights:

- **U-Net vs. SESDI On SEGSalt:** On SEGSalt, which is the ideal data set for CNN based U-Net, SESDI performs better than U-net on all the metrics with significant margin (Table 1). This begs the question of whether convolutions are apt for seismic inversion. Convolution based networks are known for their strong priors and disregard for long-range dependencies. MLPs, on the other hand, can capture all range dependencies and hence perform better. Visualizations in figure 8 also echo similar results. At times, U-Net incorrectly predicts background velocity and shows weird salt structures. Though SESDI’s output suffers from over-smoothing the boundaries, it captures the salt and background’s general shape in detail.
- **RS-SEGSalt vs. SEGSalt** Training the model on RS-SEGSalt leads to robust models due to the availability of extensive, varied data created by subsampling. Note that RS-SEGSalt only differs from SEGSalt in the input. Thus, we can train the model on RS-SEGSalt and test it on SEGSalt. We can see from figure 8 that SESDI gives better salt shapes when trained on RS-SEGSalt. This is also reflected by better  $\mathcal{L}_1$  and PSNR for SESDI.
- **SESDI vs Set-Transformer** Table 1 also

demonstrates the superiority of SESDI over set-transformer. On regular observation, SESDI achieves over 20% performance boost on set-transformer. One intuition behind this results is that there is less dependency between traces. Thus, attending one trace with others would not improve the generalization of the set model.

- **SESDI on GulfM.** Figure 7 (right), shows that we get geologically sound predictions of the velocity model by using SESDI model. The image is obtained by stitching together the individual blocks predicted by SESDI model. Figure 7 (left) shows a mixture of small block predictions. SSIM on real velocity prediction is higher than that on synthetic data. Real velocities in a small block are relatively smooth, whereas synthetic data is filled with complexities to resemble the entire survey.

## 5 Conclusion

To tackle the scale of seismic inversion, we introduce an auxiliary task of contextual small property model block prediction to solve the problem of large-scale property model (in Gigabytes) prediction from Terabytes of data. We can efficiently train models for this auxiliary task. We alleviate the issues of highly irregular geometry of acquisition by formulating the Context as a bag of informative traces and provide a SESDI model to align and combine this data. Our model achieves geologically sound predictions on real data at its original scale. We believe this is the first-ever demonstration of a model on real scale seismic data.

**Acknowledgement:** The authors thank Shell International E&P for financial support, computational resources, and permission to publish this work. The authors also thank TGS for providing the data.

## References

- Alsadi, H. N. Seismic hydrocarbon exploration. *2D and 3D Techniques, Seismic waves*, 2017.
- Araya, M., Dahlke, T., Frogner, C., Zhang, C., Poggio, T., and Hohl, D. Automated fault detection without seismic processing. *The Leading Edge*, 36: 208–214, 03 2017. doi: 10.1190/tle36030208.1.
- Araya, M., Jennings, J., Adler, A., and Dahlke, T. Deep-learning tomography. *The Leading Edge*, 37: 58–66, 01 2018. doi: 10.1190/tle37010058.1.
- Araya-Polo, M., Jennings, J., Adler, A., and Dahlke, T. Deep-learning tomography. *The Leading Edge*, 37(1):58–66, 2018.
- Arora, N. S., Russell, S. J., Kidwell, P., and Sudderth, E. B. Global seismic monitoring as probabilistic inference. In *NIPS*, pp. 73–81, 2010.
- Brossier, R., Operto, S., and Virieux, J. Seismic imaging of complex onshore structures by 2d elastic frequency-domain full-waveform inversion. *Geophysics*, 74(6):WCC105–WCC118, 2009.
- Calderon Agudo, O., Caprioli, P., and van Manen, D.-J. A spatially compact source signature filter. *GEOPHYSICS*, 81:V39–V53, 02 2016. doi: 10.1190/geo2015-0259.1.
- Cerjan, C., Kosloff, D., Kosloff, R., and Reshef, M. A nonreflecting boundary condition for discrete acoustic and elastic wave equations. *Geophysics*, 50(4):705–708, 1985.
- Chen, L.-C., Papandreou, G., Kokkinos, I., Murphy, K., and Yuille, A. L. Deeplab: Semantic image segmentation with deep convolutional nets, atrous convolution, and fully connected crfs. *IEEE transactions on pattern analysis and machine intelligence*, 40(4):834–848, 2017.
- Crout, R. L. Oil and gas platform ocean current profile data. In *OCEANS 2008*, pp. 1–9. IEEE, 2008.
- Di, H., Wang, Z., and AlRegib, G. Why using cnn for seismic interpretation? an investigation. In *SEG Technical Program Expanded Abstracts 2018*, pp. 2216–2220. Society of Exploration Geophysicists, 2018.
- Dramsich, J. S. and Luthje, M. Deep-learning seismic facies on state-of-the-art cnn architectures. In *Seg technical program expanded abstracts 2018*, pp. 2036–2040. Society of Exploration Geophysicists, 2018.
- Fichtner, A. *Full seismic waveform modelling and inversion*. Springer Science & Business Media, 2010.
- Goodfellow, I., Bengio, Y., Courville, A., and Bengio, Y. *Deep learning*, volume 1. MIT press Cambridge, 2016.
- Griffith, D. P., Zamanian, S. A., Vila, J., Vial-Aussavy, A., Solum, J., Potter, R. D., and Menapace, F. Deep learning applied to seismic attribute computation. *Interpretation*, 7(3):SE141–SE150, 2019.
- Huynh-Thu, Q. and Ghanbari, M. Scope of validity of psnr in image/video quality assessment. *Electronics letters*, 44(13):800–801, 2008.
- Julian, B. R. and Foulger, G. Earthquake mechanisms from linear-programming inversion of seismic-wave amplitude ratios. *Bulletin of the Seismological Society of America*, 86(4):972–980, 1996.
- Komatitsch, D. and Tromp, J. A perfectly matched layer absorbing boundary condition for the second-order seismic wave equation. *Geophysical Journal International*, 154(1):146–153, 2003.
- Le Ravalec, M., Tillier, E., Da Veiga, S., Enchéry, G., and Gervais, V. Advanced integrated workflows for incorporating both production and 4d seismic-related data into reservoir models. *Oil & Gas Science and Technology—Revue d’IFP Energies nouvelles*, 67(2):207–220, 2012.
- Lee, J., Lee, Y., Kim, J., Kosiorek, A., Choi, S., and Teh, Y. W. Set transformer: A framework for attention-based permutation-invariant neural networks. In *International Conference on Machine Learning*, pp. 3744–3753. PMLR, 2019.
- Li, X. R., Mitsakos, N., Lu, P., Xiao, Y., Zhan, C., and Zhao, X. Generative inpainting network applications on seismic image compression and non-uniform sampling. In *Workshop on Solving Inverse Problems with Deep Networks, NeurIPS*, 2019.
- Lin, Y. and Huang, L. Acoustic-and elastic-waveform inversion using a modified total-variation regularization scheme. *Geophysical Journal International*, 200(1):489–502, 2014a.
- Lin, Y. and Huang, L. Ultrasound waveform tomography with a spatially variant regularization scheme. In *Medical Imaging 2014: Ultrasonic Imaging and Tomography*, volume 9040, pp. 90401M. International Society for Optics and Photonics, 2014b.

- Lin, Y. and Huang, L. Quantifying subsurface geophysical properties changes using double-difference seismic-waveform inversion with a modified total-variation regularization scheme. *Geophysical Supplements to the Monthly Notices of the Royal Astronomical Society*, 203(3):2125–2149, 2015.
- Louboutin, M., Lange, M., Luporini, F., Kukreja, N., Witte, P. A., Herrmann, F. J., Velesko, P., and Gorman, G. J. Devito (v3.1.0): an embedded domain-specific language for finite differences and geophysical exploration. *Geoscientific Model Development*, 12(3):1165–1187, 2019. doi: 10.5194/gmd-12-1165-2019. URL <https://www.geosci-model-dev.net/12/1165/2019/>.
- Luporini, F., Lange, M., Louboutin, M., Kukreja, N., Hückelheim, J., Yount, C., Witte, P., Kelly, P. H. J., Herrmann, F. J., and Gorman, G. J. Architecture and performance of devito, a system for automated stencil computation. *CoRR*, abs/1807.03032, jul 2018. URL <http://arxiv.org/abs/1807.03032>.
- Mandelli, S., Lipari, V., Bestagini, P., and Tubaro, S. Interpolation and denoising of seismic data using convolutional neural networks. *arXiv preprint arXiv:1901.07927*, 2019.
- Nath, S. K., Chakraborty, S., Singh, S. K., and Ganguly, N. Velocity inversion in cross-hole seismic tomography by counter-propagation neural network, genetic algorithm and evolutionary programming techniques. *Geophysical Journal International*, 138(1):108–124, 1999.
- Nolet, G. Seismic wave propagation and seismic tomography. In *Seismic tomography*, pp. 1–23. Springer, 1987.
- Onajite, E. *Seismic data analysis techniques in hydrocarbon exploration*. Elsevier, 2013.
- Özdenvar, T. and McMechan, G. A. Algorithms for staggered-grid computations for poroelastic, elastic, acoustic, and scalar wave equations. *Geophysical Prospecting*, 45(3):403–420, 1997.
- Rojas-Gómez, R., Yang, J., Lin, Y., Theiler, J., and Wohlberg, B. Physics-consistent data-driven waveform inversion with adaptive data augmentation. *IEEE Geoscience and Remote Sensing Letters*, 2020.
- Ronneberger, O., Fischer, P., and Brox, T. U-net: Convolutional networks for biomedical image segmentation. In *International Conference on Medical image computing and computer-assisted intervention*, pp. 234–241. Springer, 2015.
- Sergeant, A., Mangeney, A., Stutzmann, E., Montagner, J.-P., Walter, F., Moretti, L., and Castelnau, O. Complex force history of a calving-generated glacial earthquake derived from broadband seismic inversion. *Geophysical Research Letters*, 43(3): 1055–1065, 2016.
- Shapiro, N. M., Campillo, M., Stehly, L., and Ritzwoller, M. H. High-resolution surface-wave tomography from ambient seismic noise. *Science*, 307(5715):1615–1618, 2005.
- Sun, Y., Denel, B., Daril, N., Evano, L., Williamson, P., and Araya-Polo, M. Deep learning joint inversion of seismic and electromagnetic data for salt reconstruction. In *SEG Technical Program Expanded Abstracts 2020*, pp. 550–554. Society of Exploration Geophysicists, 2020.
- Van Der Neut, J., Tatanova, M., Thorbecke, J., Slob, E., and Wapenaar, K. Deghosting, demultiple, and deblurring in controlled-source seismic interferometry. *International Journal of Geophysics*, 2011, 2011.
- Virieux, J. and Operto, S. An overview of full-waveform inversion in exploration geophysics. *Geophysics*, 74(6):WCC1–WCC26, 2009.
- Wang, Z., Bovik, A. C., Sheikh, H. R., and Simoncelli, E. P. Image quality assessment: from error visibility to structural similarity. *IEEE transactions on image processing*, 13(4):600–612, 2004.
- Waters, K. H. and Waters, K. H. *Reflection seismology: A tool for energy resource exploration*. Wiley New York, NY, 1981.
- Wu, Y. and Lin, Y. Inversionnet: A real-time and accurate full waveform inversion with cnns and continuous crfs. *arXiv: Signal Processing*, 2018.
- Xie, X.-B. and Yang, H. The finite-frequency sensitivity kernel for migration residual moveout and its applications in migration velocity analysis. *Geophysics*, 73(6):S241–S249, 2008.
- Yang, F. and Ma, J. Deep-learning inversion: a next generation seismic velocity-model building method. *ArXiv*, abs/1902.06267, 2019.
- Yilmaz, Ö. *Seismic data analysis: Processing, inversion, and interpretation of seismic data*. Society of exploration geophysicists, 2001.

- Zaheer, M., Kottur, S., Ravanbakhsh, S., Póczos, B., Salakhutdinov, R., and Smola, A. J. Deep sets. *CoRR*, abs/1703.06114, 2017. URL <http://arxiv.org/abs/1703.06114>.
- Zelt, C. A., Azaria, A., and Levander, A. 3d seismic refraction travelttime tomography at a groundwater contamination site. *Geophysics*, 71(5):H67–H78, 2006.
- Zheng, Y., Zhang, Q., Yusifov, A., and Shi, Y. Applications of supervised deep learning for seismic interpretation and inversion. *The Leading Edge*, 38(7):526–533, 2019.

## A Experiment Details

### A.1 Seismic Data Simulation

The 2D SEG salt models in SEGSalt dataset Yang & Ma (2019) are identical to each other. The data statistics are shown in Table 2. Yang & Ma (2019) assume that the velocities varies from 2000 m/s to 4500 m/s, where the material with 4500 m/s is the salt body Onajite (2013). The shape of the target velocity matrix is  $201 \times 301$  with a spatial interval of 10m.

The simulation parameters for trace generation are shown in Table 3. We perform a the time-domain stagger-grid finite-difference scheme to simulate traces by acoustic wave equation. The scheme contains both a second-order time direction and eighthorder space direction Özdenvar & McMechan (1997). For acquisition geometry, we assume there exists 301 receivers that are uniformly distributed at a constant spatial interval. There also exists a perfectly matched layer (PML) Komatitsch & Tromp (2003) absorbing boundary condition that reduces unphysical reflection on edges. Therefore, the trace is a 2000 dimensional vector and each velocity matrix corresponds to  $29 \times 301$  traces. To fit the requirements of the CNN, each trace is down-sampled to 400 dimension by Yang & Ma (2019). Then, the 301 traces of each shot formulate a  $301 \times 400$  matrix. Therefore, the U-Net operations can performed on  $301 \times 400 \times 29$  image. Our SESDI model formulate each sample as a set with size  $n < 29 \times 301$  and element dimensionality 400. We sub-sample the  $29 \times 301$  traces to generate set embedding and predict the target velocity matrix.

Table 2: Data Statistics for 2D VMB

Dataset	Training Samples	Testing Samples	Velocity Shape
SEGSalt	130	10	$201 \times 301$
GulfM-10	400	100	$17 \times 20 \times 50$
GulfM-20	400	100	$17 \times 20 \times 100$

Table 3: Simulation Parameters

Number of Source	Number of Receivers	Sampling Frequency	Ricker Wave	Simulation Time	Traces Length
29	301	1kHz	25Hz	2s	2000

### A.2 Network Architecture

We present the SESDI network architecture on Table 4. The trace input is first embedded as a 10240 dimension vector and then pass through a 3 layer MLP. The location information is embedded as a 512 dimension vector by a 4 layer MLP. Then, the location embedding is concatenated with the trace hidden vector and all the  $n$  trace-location vectors are summed together. Finally, a hidden layer and an output layer are used to generate the final velocity matrix. All the MLP in this model are associated with ReLU activation. For set transformer Lee et al. (2019), we implement an encoder with a stack of set attention blocks. Then, we introduce a pooling by multihead attention module. Finally, we have a stack of set attention blocks in decoder. We set the dimensionality of all hidden layers to 4096 and the number of attention heads to 4.

### A.3 GulfM Dataset

The GulfM dataset is generated from the real marine survey data shared by one of the major energy and petrochemical company. As shown in the name, the raw seismic data is obtained by oil and gas platform Crout (2008) in the gulf of mexico. The large ground-truth 3D velocity models are generated by geophysicists with

Table 4: SESDI Network Architecture 2D VMB

Layer	Type	Input Dim	Hidden Units
Trace Emb	1 Layer MLP	400	10240
Trace Hidden	3 Layer MLP	10240	4096
Location Emb	4 Layer MLP	2	512
Hidden	5 Layer MLP	4096+512	4096
Output	1 Layer MLP	4096	201×301

duration over 8 months. We focus on the velocity cubes in 100m to 200m below the surface and random sample cubes within 33000m × 78000m area. In other words, we random sample velocity 1000m × 1000m × 50m and 1000m × 1000m × 100 cubes from a large 33000m × 78000m × 100m cubes to generate labels for GulfM-10 and GulfM-20 dataset. After discretization, the output velocity shapes for two GulfM datasets are 17m × 20m × 50m and 17m × 20m × 100. Then, for each velocity cubes, we acquire its corresponding traces collected on the 1000m × 1000m surface area as SESDI model’s input. Because the complex acquisition geometry, the maximum number of receivers for each trace is 7008. And the each velocity cube has traces varies from 2 to 8779. This set format prohibit convolution models in this task.

#### A.4 Model Training

We train both SESDI model and U-Net on a server with 1 Nvidia Tesla V100 GPU and two 20-core/40-thread processors (Intel Xeon(R) E5-2698 v4 2.20GHz). SESDI, set transformer and U-Net use Adam as optimizer. The training hyper-parameters for SESDI, U-Net and set transformer follow the FCNVMB paper Yang & Ma (2019) with learning rate modifications to make better performance.

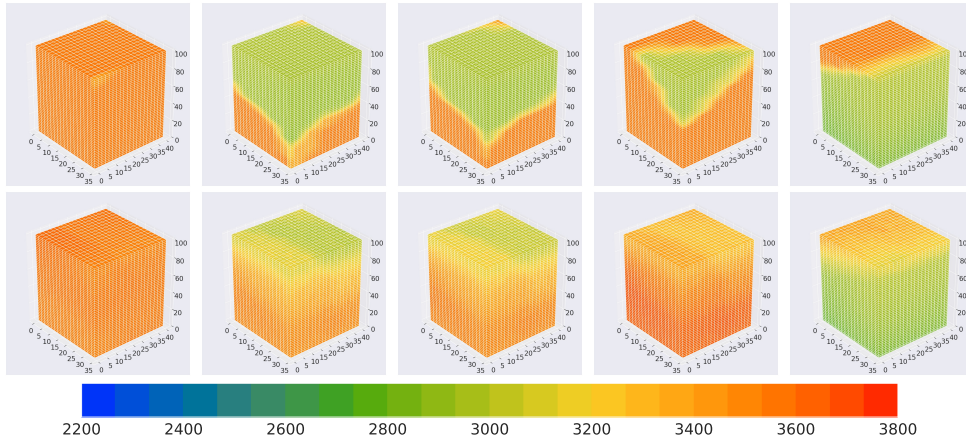


Figure 10: Visualization of Prediction on GulfM-10 Dataset. Seismic data courtesy of TGS.

#### A.5 Visualizations

We present the visualization of all predictions in SEGSalt dataset in Figure 11. A sample prediction for GulfM-10 and GulfM-20 dataset is shown in Figure 10 and Figure 12. Here, we choose different color maps for demonstrate the details information in seismic velocities. For the inference on large scale in Figure 13, we run the model in the region where both GulfM10 and GulfM20 datasets are randomly sample from.

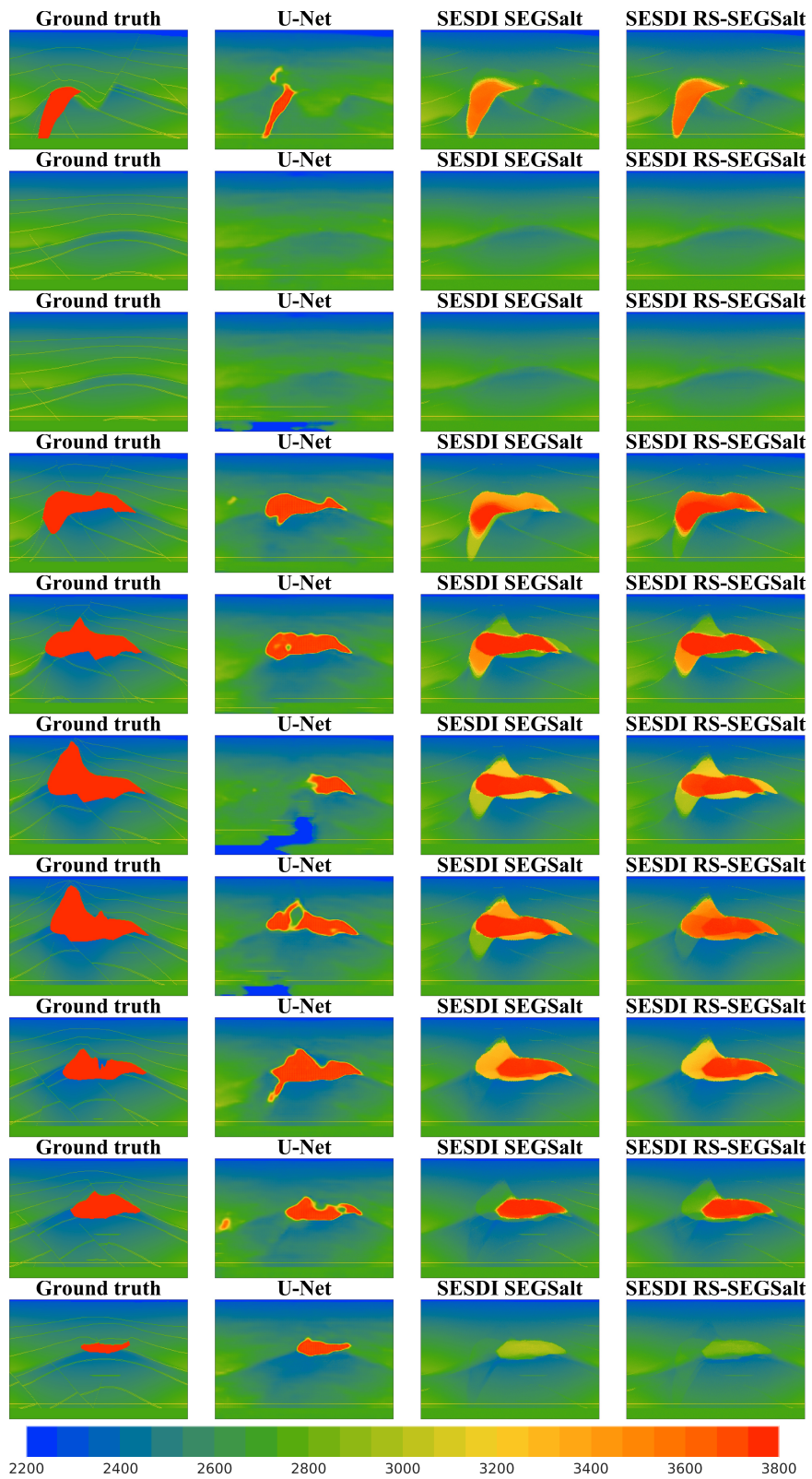


Figure 11: Visualization of Prediction on SEGSalt Dataset

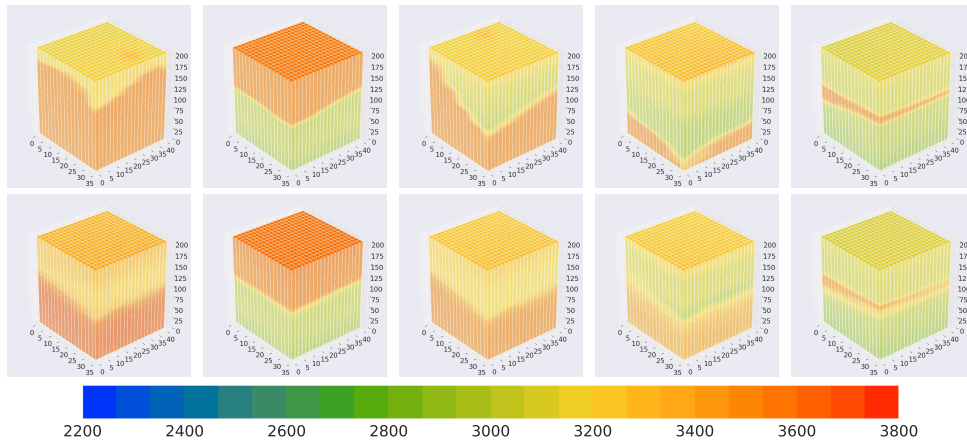


Figure 12: Visualization of Prediction on GulfM-20 Dataset. Seismic data courtesy of TGS.

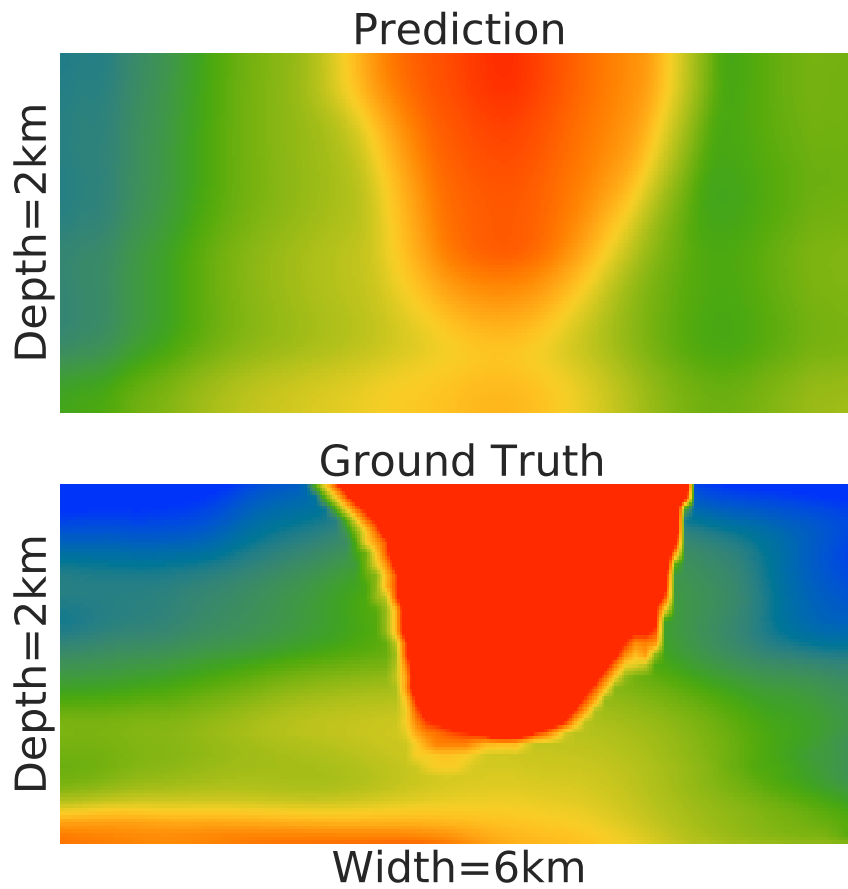


Figure 13: Visualization of Prediction on Large Scale VMB in a depth 2km and width 6km area. Seismic data courtesy of TGS.